Computer modeling and Brillouin scattering studies of anharmonicity and high-temperature disorder in LaF_3

P. E. Ngoepe
Department of Physics, University of the North, Sovenga 0727, South Africa

W. M. Jordan
Department of Chemistry, University College, London, 20 Gordon Street, London WC1H 0AJ, United Kingdom

C. R. A. Catlow
Department of Chemistry, University of Keele, Keele, Staffordshire ST5 5BG, United Kingdom

J. D. Comins
Department of Physics, University of the Witwatersrand, Johannesburg, P.O. Wits 2050, South Africa
(Received 29 August 1989)

Brillouin scattering studies of LaF_3 at high temperatures have yielded the complete set of acoustic-mode frequencies associated with the elastic constants. These show a linear decrease with temperature up to about 1150 K, this being associated with lattice expansion. Above 1150 K, the elastic constants show a marked reduction with the exception of C_{44}, which remains nearly constant. This behavior, which results from a diffuse superionic transition to a disordered state, has been computationally simulated by energy-minimization techniques. The nature of the dominant high-temperature disorder has been examined with the use of a supercell approach to permit appropriate defect concentrations and types. The calculations favor anion Frenkel disorder in an estimated concentration of 2 mole % at 1400 K.

I. INTRODUCTION

Superionic, or fast-ion, conductors have received considerable attention in the past 15 years owing to their applications as solid electrolytes in energy-storage devices and ion-specific electrodes. Computer modeling[1-4] and a number of experimental techniques[5,6] have made notable contributions to our understanding of the rather complex defect processes involved particularly in the case of fluorite-structure compounds.

The current theoretical understanding of fluorites involves the development of significant, but limited anion Frenkel disorder resulting from a diffuse phase transition to the superionic state. A crucial feature of the model of this transition is the presence of a defect interaction term in the free energy causing a reduction in the effective Frenkel-defect-formation energy.[1] The presence of these relatively large concentrations of defects causes inter alia a substantial rise in ionic conductivity, an anomalous increase in specific heat,[5,6] and a significant reduction in certain elastic constants in the region of a transition temperature T_c.[7-10] The latter effect has been computationally simulated in fluorites and permits an estimate of the defect concentration.[7]

Recently interest in the elastic properties of superionics has been extended to the light-lanthanide trifluorides (MF_3) with the tysonite crystal structure.[11-13] As demonstrated by ionic conductivity and NMR studies on LaF_3 and CeF_3, these compounds differ from the fluorites in that they are moderately good ionic conductors even at ambient temperature.[14-19] The controversy concerning the relative mobilities of fluorine ions on the different sublattices[19,20] was recently clarified by a computer simulation study of LaF_3.[21] This favors predominant fluorine motion in planes perpendicular to the c axis. The model also assumes a substantial fluorine-vacancy concentration.

The nature of the predominant type of disorder in LaF_3 has been a subject of controversy. Lattice parameter and dilatation measurements suggest Schottky disorder.[22] However, recent computer simulation studies indicate a lower formation energy for anion Frenkel rather than Schottky defects.[21] It should be pointed out that both results refer to temperatures below 1000 K.

Evidence to support thermally induced disorder at yet higher temperatures in LaF_3 and CeF_3 is now emerging. Although several ionic conductivity studies have been reported,[14,15,20,23] it is only recently that measurements have been extended from 1000 to 1500 K.[24] A significant conductivity increase occurs above 1150 K, followed by a slight reduction in the rate of increase above 1500 K. Furthermore, a substantial excess specific-heat increase is observed above the same temperature.[25] Brillouin scattering studies have shown significant reductions in certain acoustic mode frequencies and the associated elastic constants in LaF_3 and CeF_3 above 1150 K.[12,13] As discussed above, such elastic anomalies are associated with a diffuse transition to the superionic state in fluorites.

In this article we report acoustic mode frequencies related to the complete set of elastic constants for temperatures approaching 1500 K as measured by the Brillouin scattering method. Furthermore, we calculate elastic constants using computer modeling techniques; we investigate the effects both of lattice expansion and the presence of anion Frenkel and Schottky disorder. A comparison of these experimental and theoretical results is used to predict the dominant species of disorder and its concentration at high temperatures. In Sec. II we introduce the model and the simulation method used in the calculations, Section III describes the experimental procedures. In Sec. IV we present the experimental and theoretical results. Discussions and conclusions are provided in Sec. V.

II. THEORETICAL CONSIDERATIONS

A. Structure and defect energies

Studies of the structure of LaF_3 have suggested various space groups which subsequently have been reduced to two possibilities. The first proposal has hexagonal symmetry with a $P6_3cm$ space group[26] and is characterized by four inequivalent fluorine sublattices in the ratio 2:4:6:6 (Fig. 1). An alternative structure has trigonal symmetry with the $P\bar{3}c1$ space group[19,27] and has three inequivalent fluorine sites in the ratio 2:4:12; as shown in

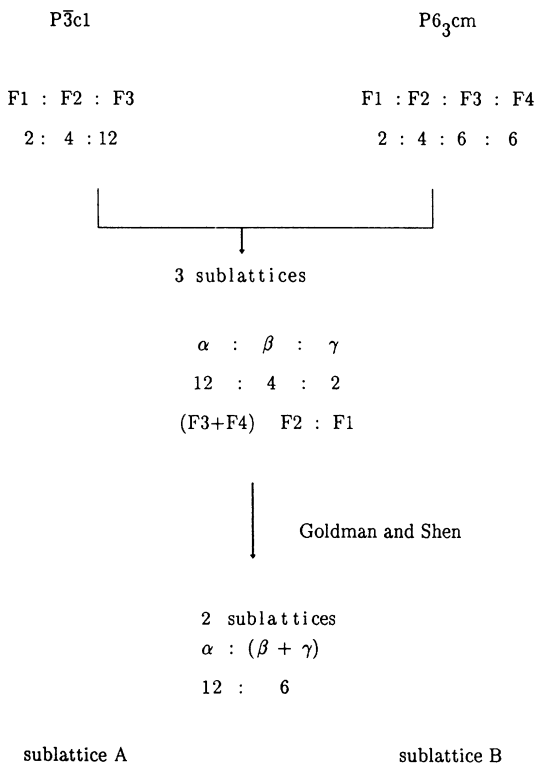

FIG. 1. Fluorine sublattice models in LaF_3.

TABLE I. The atomic parameters of LaF_3 in the $P\bar{3}c1$ space group. Lattice parameter: $a=7.185$ Å, $c=7.351$ Å. X and Y are expressed in terms of a; Z is expressed in terms of c.

Atom	X	Y	Z
La	0.6602	0.0000	0.2500
F(1)	0.0000	0.0000	0.2500
F(2)	0.3333	0.6667	0.1867
F(3)	0.3659	0.0537	0.0814

Fig. 1, the Goldman-Shen model[17] simplifies the structure to one with sublattices A and B. In both space groups the structure is heximolecular with six formula units per unit cell. The difference in atomic coordinates or bond lengths is small and calculated defect energies are similar. The $P\bar{3}c1$ space group was chosen in this study and the atomic parameters are given in Table I. Anion Frenkel and Schottky defect formation energies for defects created on the different sublattices are given in Table II, using the results of Jordan and Catlow.[21]

B. Computational procedure

Perfect lattice elastic constants were calculated by the standard procedures available in the THBREL code which is closely related to the PLUTO program written by Catlow and Norgett.[28] The variation of the elastic constants with temperature was simulated by allowing the lattice parameter to vary in accordance with the experimentally determined thermal-expansion coefficient.[22]

For crystals containing defects, supercell calculations were performed in the determination of lattice energies and elastic constants. The method entails setting up a supercell comprising the defect and its surrounding lattice and repeating it infinitely in space. We constructed supercells containing 2, 3, 4, 6, and 8 basic unit cells of LaF_3. For Frenkel defect supercells an anion Frenkel pair consisting of an interstitial site of type 3 (defined in Table II) and a fluorine-ion vacancy of type F3 (defined in Table I) were chosen. This combination results in the lowest Frenkel defect formation energy as shown in Table II. The fluorine-ion vacancy and interstitial were located in different unit cells to avoid their recombination during energy minimization. In the case of the Schottky defect supercell (Table II) fluorine-ion vacancy positions nearest to a lanthanum ion were chosen; i.e., a bound Schottky quartet was studied. The concentration of defects in the lattice was diluted by increasing the size of the supercell around a single anion Frenkel pair or Schottky quartet (see Table VI). Furthermore, these calculations also enabled the defect interaction energy to be investigated as a function of defect separation.

The energy-minimization procedure was applied using the THBREL code on the lattice containing defects until equilibrium configurations were achieved. In our computations, lattice vectors were kept constant (constant volume), and only atomic coordinates were adjusted for zero strain. The lattice energies corresponding to different defect concentrations were calculated and elastic constants were determined from the derivatives of these

TABLE II. The anion Frenkel and Schottky defect formation energies in LaF_3 [after Jordan and Catlow (Ref. 21)].

Anion Frenkel model: Calculated formation energies			
F^- Interstitial site	F^--interstitial formation energy (eV)	F^--vacancy site	Frenkel-pair-formation energy (eV)
(1) 0.6629 0.8660 0.4600	0.22	F(1)	3.20
		F(2)	3.49
		F(3)	2.82
(2) 0.1276 0.4660 0.4800	−0.26	F(1)	2.72
		F(2)	3.01
		F(3)	2.34
(3) 0.2500 0.1443 0.5115	−0.33	F(1)	2.65
		F(2)	2.94
		F(3)	2.27

Experimental Frenkel formation energy: 1 eV

Schottky model		
vacancy site	Calculated formation energy (eV)	Calculated Schottky formation energy (eV)
F(1)	2.98	6.78
F(2)	3.27	7.65
F(3)	2.60	5.64
La	46.68	5.64

Experimental Schottky formation energy: 2 eV

energies with respect to atomic coordinates.

The interatomic potentials used in this study are those of Jordan and Catlow.[21] The lattice energy is the sum of Coulomb and short-range terms, the latter cast in the form of a Buckingham potential,

$$V_{ij}(r)=A_{ij}\exp(-r_{ij}/\rho_{ij})-C_{ij}/r_{ij}^6 . \quad (1)$$

For the Coulomb interactions, the effective charges were assigned their full normal values and the lattice summations were achieved by the Ewald procedure. The short-range terms were handled in real space and had a cutoff distance of 9.78 Å. The treatment of ionic polarizability was based on the shell model of Dick and Overhauser[29] and expressed in terms of the respective shell charges Y and spring constants k for the La^{3+} and F^- ions. The values of the parameters used for the short-range interionic potentials and shell model appear in Table III.

TABLE III. The parameters for the short-range interionic potentials and those for the shell model.

Short-range interaction potential parameters			
	A_{ij} (eV)	ρ_{ij} (Å)	C_{ij} (eV Å^{-6})
La^{3+}-La^{3+}	53 317.7	0.2206	0
La^{3+}-F^-	1476.86	0.3252	0
F^--F^-	1127.70	0.2753	15.83

Short-range potential cutoff distance: 9.78 Å

Shell model parameters		
	$Y/\lvert e\rvert$	k (eV Å^{-2})
La^{3+}	6.59	250.0
F^-	−2.38	101.2

III. EXPERIMENTAL METHODS

Brillouin spectra were excited using the 514.5-nm line of an argon-ion laser, operated in a single axial mode. The light scattered by 90° was analyzed by a triple-pass, piezoelectrically scanned Fabry-Perot interferometer, which was electronically stabilized. The signals were detected by a photomultiplier and phonon counting system used in conjunction with a multichannel analyzer.

The frequency shift in Brillouin scattered light is given by

$$\Delta\omega_B=\frac{v\omega_0}{c}(n_i^2+n_s^2-2n_in_s\cos\theta) . \quad (2)$$

The refractive indices n_i and n_s are defined for the directions of the incident and scattered light where the scattering angle is θ. Optical isotropy may be assumed in LaF_3 as n_i and n_s differ by only 0.4%.[11] Since birefringence effects are so small, Eq. (2) reduces to

$$\Delta\omega_B=(2\bar{n}v\omega_0/c)\sin(\theta/2) , \quad (3)$$

where v is the velocity of the acoustic phonons causing the light scattering, $\bar{n}=(n_i+n_s)/2$, ω_0 is the frequency of the incident light, and c is the velocity of light. Table VII(a) gives the phonon propagation directions together with the modes used. **K** is the unit vector parallel to the phonon propagation direction; **u** is the phonon polarization direction with its components u_k^i being in some cases

complicated experssions involving elastic constants [Table VII(b)]; γ_{ij} are the relevant combinations of elastic constants; and L, QL, QT, and T refer to the longitudinal, quasilongitudinal, quasitransverse, and pure transverse modes, respectively. In view of the equivalence of the phonon velocity in the (1,0,0) and (0,1,0) directions, and that $C_{14} \simeq 0$,[11] the hexagonal approximation to trigonal symmetry is assumed. From Eq. (3), if $\bar{n}^2/\rho$ is considered slowly varying, as in fluorite structured compounds,[8] then $(\Delta\omega_B)^2$ is proportional to the appropriate elastic constant combination γ_{ij}.

Three samples of LaF_3 were oriented using the Laue x-ray backreflection technique. They were cut into cubes of approximate edge dimension 3.5 mm using a wire saw and polished to a 6-μm finish. In order to minimize contamination of the polished surfaces at high temperatures, the samples were encapsulated under ultrapure argon gas in fused silica capsules. A recess, cut ultrasonically in the base of the capsule and matched to the sample dimensions, ensured that the sample orientation within the capsule was maintained. The sample capsules were mounted in an optical furnace[30] and accurately aligned with respect to the incident laser beam.

IV. RESULTS

The squares of the acoustic mode frequencies $(\Delta\omega_B)^2$, associated with elastic constants or their combinations, were obtained from light scattering by phonons propagating along (1,0,0,), $(0,1,1)/\sqrt{2}$, and $(-1,\sqrt{2},1)/2$ directions [Table VII(a)]. Figure 2 gives the temperature variation of $(\Delta\omega_B)^2$ for the quasilongitudinal γ_{13} (QL), quasitransverse γ_{14} (QT), and pure transverse γ_{15} (T) modes in

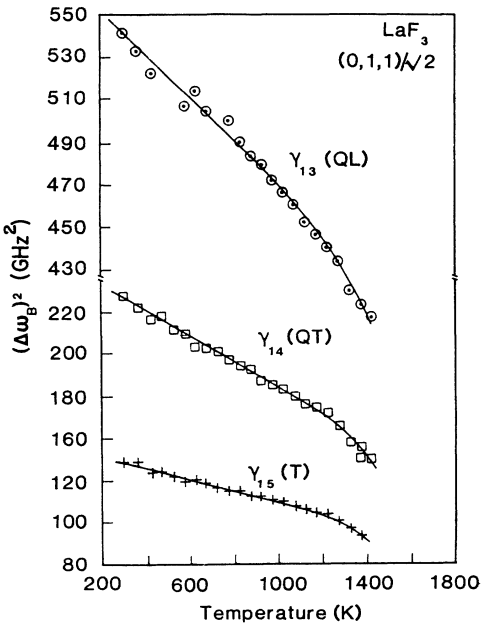

FIG. 2. The variation with temperature of the squares of Brillouin frequency shifts $(\Delta\omega_B)^2$ for the different acoustic modes of LaF_3 in the $(0,1,1)/\sqrt{2}$ direction.

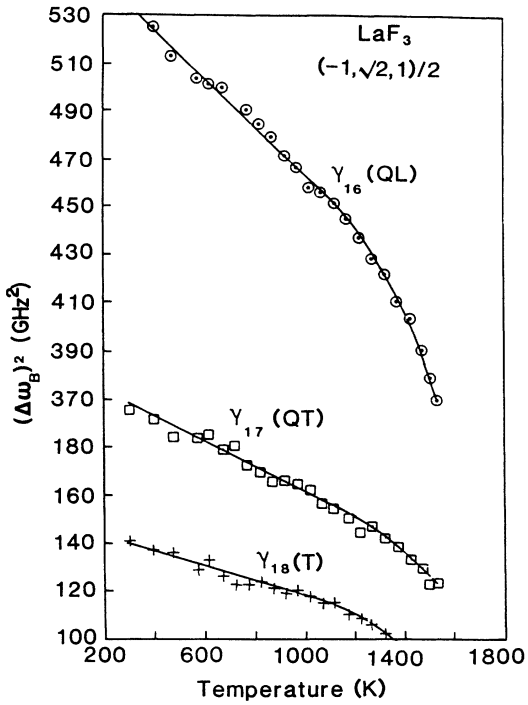

FIG. 3. The variation with temperature of $(\Delta\omega_B)^2$ for the different acoustic modes of LaF_3 in the $(-1,\sqrt{2},1)/2$ direction.

the $(0,1,1)/\sqrt{2}$ direction. Similar measurements on modes γ_{16} (QL), γ_{17} (QT), and γ_{18} (T), carried out in the $(-1,\sqrt{2},1)/2$ direction, are presented in Fig. 3. Figure 4(a) reflects $(\Delta\omega_B)^2$, related to C_{11}, as a function of temperature and was obtained from the (1,0,0) phonon propagation direction. Scattering from the transverse acoustic modes in this direction was too weak to be observed. Direct measurements of $(\Delta\omega_B)^2$ associated with C_{33} were unsuccessful, since excessive scattering of parasitic light occured for the (0,0,1) phonon propagation direction. Hence $(\Delta\omega_B)^2$ related to C_{33} was calculated from the measured modes shown in Figs. 2 and 3, making use of the relations in Table VII(a). The temperature dependence of C_{33} is shown in Fig. 4(a). In order to relate these observations to the behavior of the specific-heat capacity as determined by Lyon *et al.*,[25] the excess specific-heat capacity ΔC_p was calculated from their data

TABLE IV. A comparison of the calculated and experimental temperature gradients of the various elastic constants below 1100 K.

C_{ij}	dC_{ij}/dT (MPa/K) Experimental	Calculated
C_{11}	34.4	37.2
C_{33}	48.8	34.8
C_{13}	5.4	7.6
C_{66}	10.4	13.0
C_{44}	6.7	7.6

TABLE V. A comparison of the experimental percentage changes of elastic constants above 1150 K and those calculated on the basis of the anion Frenkel and Schottky models.

	Experimental 1400 K %	Frenkel model 2 mol % %	Schottky model 2 mol % %
$(\Delta C_{11})/C_{11}$	3.7	6.9	8.4
$(\Delta C_{33})/C_{33}$	4.4	4.4	8.0
$(\Delta C_{13})/C_{13}$	10.2	10.1	11.7
$(\Delta C_{66})/C_{66}$	11.0	11.1	12.0
$(\Delta C_{44})/C_{44}$	0.0	−3.0	15.8

as the difference between the experimental and Debye values and expressed as a function of temperature in Fig. 4(b).

All directly measured mode frequencies show a common pattern; a linear decrease of $(\Delta\omega_B)^2$ with temperature up to 1150 K, followed by a marked softening up to 1500 K. The anomalous increase in ΔC_p above about 1100 K in Fig. 4(b) coincides with the additional reduction of $(\Delta\omega_B)^2$. The linear changes of C_{11} and C_{33} have been extended beyond 1150 K in Fig. 4(a) for comparison with the theoretical calculations.

The measured $(\Delta\omega_B)^2$ in Figs. 2 and 3 were also used to calculate $(\Delta\omega_B)^2$ corresponding to the individual elastic constants C_{11}, C_{13}, C_{66}, and C_{44} for LaF_3 which are shown in Fig. 5. A comparison of the measured (Fig. 4) and calculated (Fig. 5) values of C_{11} shows a most satisfactory degree of agreement if we consider the large number of modes used and the complexity of the relations shown in Table VII(a). It is again noted, in Fig. 5, that all $(\Delta\omega_B)^2$ change linearly with temperature below 1150 K and those related to C_{11}, C_{13}, and C_{66} suffer an additional reduction above this temperature. However, the

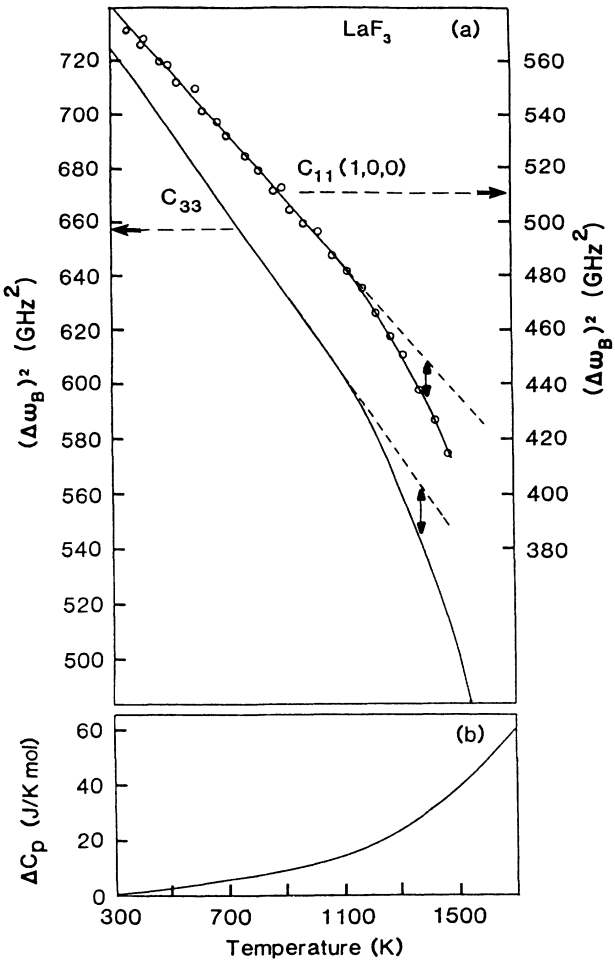

FIG. 4. (a) The temperature dependence of $(\Delta\omega_B)^2$ related to the directly measured C_{11} for the (1,0,0) phonon propagation direction; the calculated temperature dependence of C_{33} determined from modes shown in Figs. 2 and 3. (b) ΔC_p, the difference between the experimental and Debye heat capacities for LaF_3 as a function of temperature as determined from the data of Ref. 25.

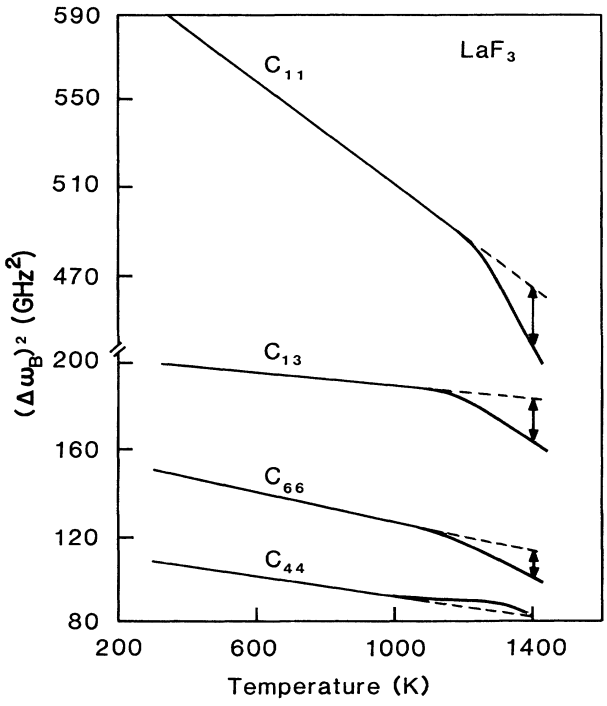

FIG. 5. The temperature variation of $(\Delta\omega_B)^2$ corresponding to the individual elastic constants C_{11}, C_{13}, C_{66}, and C_{44}.

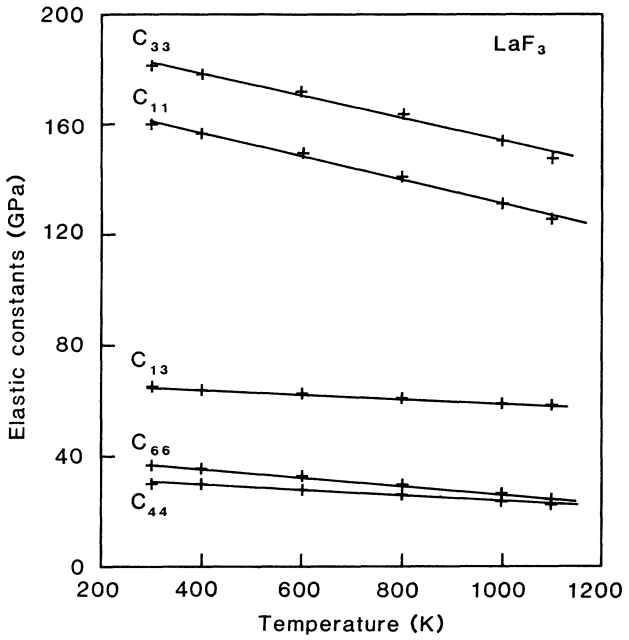

FIG. 6. The variation of elastic constants with temperature, calculated by allowing the lattice to expand with temperature.

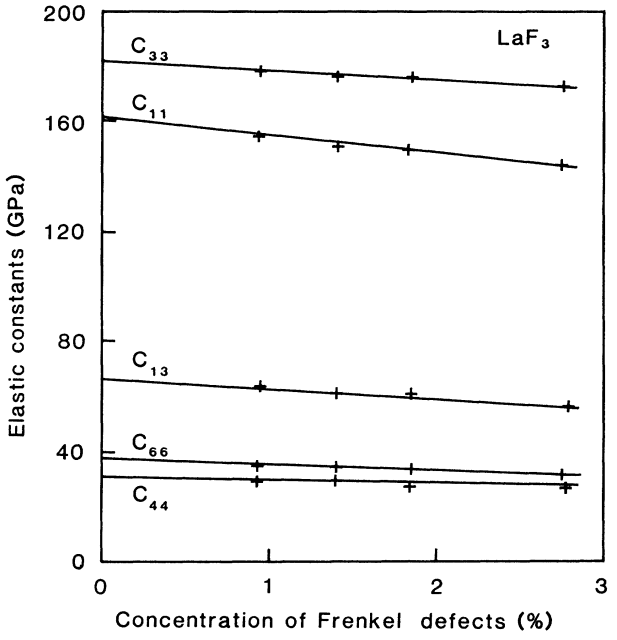

FIG. 7. The calculated change of elastic constants of LaF_3 with increasing concentration of anion Frenkel disorder.

behavior of $(\Delta\omega_B)^2$ related to C_{44} is significantly different from the others in that there is a near constancy of dC_{44}/dT above 1150 K, followed by a small decrease above 1300 K.

Theoretical calculations of elastic constants for the perfect lattice based on lattice expansion (see Sec. II B) are given in Fig. 6. All elastic constants vary linearly with temperature up to about 1100 K. A comparison of experimental and theoretical temperature gradients of elastic constants is given in Table IV. Although discrepancies occur in the absolute values of calculated and experimental elastic constants, the main features are quite satisfactory.

Computer simulation results based on the anion Frenkel and Schottky models (see Sec. II B) are presented in Figs. 7 and 8, respectively. In Fig. 7 for Frenkel defects all elastic constants reduce with increasing defect content, *with the exception of C_{44}, which tends to a constant value.* However, in the case of the Schottky model (Fig. 8) all elastic constants decrease with the concentration of defects.

Table V features precentage deviations of the experimental elastic constants from the extrapolated anharmonic values at 1400 K. These results compare favorably with calculations based on the anion Frenkel model where the concentration of defects is estimated at 2%. In particular, the near constancy of C_{44} is reproduced. The agreement with the Schottky model is less satisfactory,

TABLE VI. Energies associated with defect supercells in LaF_3. Asterisk denotes zero-value result from recombination during energy minimization.

		Frenkel model		Schottky model	
Supercell size unit cells	Perfect lattice energy (eV)	Defect concentration (%)	Defect interaction energy (eV)	Defect concentration (%)	Defect interaction energy (eV)
1	−293.05	5.56	0*	16.60	
2	−586.10	2.78	0.70	8.30	
3	−879.15	1.85	0.49	5.56	
4	−1172.20	1.39	0.44	4.17	2.92
6	−1758.30	0.93	0.35	2.78	2.60
8	−2344.40	0.47		2.09	

Frenkel pair defect formation energy 2.27 eV
Schottky quartet defect formation energy 5.64 eV

particularly in the behavior of C_{44}, which is the most critical case; here a relatively large fractional decrease of 15.8% in $\Delta C_{44}/C_{44}$ is calculated.

Table VI shows sizes of the various supercells, their perfect lattice energies, corresponding concentrations of Frenkel and Schottky disorder, and defect interaction energies (see also Sec. II B). It is observed that in both models defect interaction energies increase with the con-

TABLE VII. (a) Combinations of elastic constants of a hexagonal crystal in the various phonon propagation and polarization directions. (b) Phonon polarization vector components u_k^i corresponding to (a).

(a)

K	u	Mode	γ_{ij}
(1,0,0)	(1,0,0)	L	C_{11}
(0,0,1)	(0,0,1)	L	C_{33}
$(0,1,1)/\sqrt{2}$	$(0,u_2^3,u_3^3)$	QL	γ_{13}
$(0,1,1)/\sqrt{2}$	$(0,u_2^4,u_3^4)$	QT	γ_{14}
$(0,1,1)/\sqrt{2}$	(1,0,0)	T	γ_{15}
$(-1,\sqrt{2},1)/2$	(u_1^5,u_2^5,u_3^5)	QL	γ_{16}
$(-1,\sqrt{2},1)/2$	(u_1^6,u_2^6,u_3^6)	QT	γ_{17}
$(-1,\sqrt{2},1)/2$	$(1,0,1)/\sqrt{2}$	T	γ_{18}

$$\gamma_{13}=\tfrac{1}{4}\{C_{33}+C_{11}+2C_{44}+[(C_{11}-C_{33})^2+4(C_{13}+C_{44})^2]^{1/2}\}$$
$$\gamma_{14}=\tfrac{1}{4}\{C_{33}+C_{11}+2C_{44}-[(C_{11}-C_{33})^2+4(C_{13}+C_{44})^2]^{1/2}\}$$
$$\gamma_{15}=(C_{44}+C_{66})/2$$
$$\gamma_{16}=\tfrac{1}{4}\{3C_{11}+C_{33}+4C_{44}+[(3C_{11}-2C_{44}-C_{33})^2+12(C_{13}+C_{44})^2]^{1/2}\}$$
$$\gamma_{17}=\tfrac{1}{4}\{3C_{11}+C_{33}+4C_{44}-[(3C_{11}-2C_{44}-C_{33})^2+12(C_{13}+C_{44})^2]^{1/2}\}$$
$$\gamma_{18}=(C_{44}+3C_{66})/4$$

(b)

$$u_2^3=(C_{13}+C_{44})[(2\gamma_{13}-C_{11}-C_{44})^2+(C_{13}+C_{44})^2]^{-1/2}$$
$$u_3^3=-(2\gamma_{13}-C_{11}-C_{44})[(2\gamma_{13}-C_{11}-C_{44})^2+(C_{13}+C_{44})^2]^{-1/2}$$
$$u_2^4=(C_{13}+C_{44})[(2\gamma_{14}-C_{11}-C_{44})^2+(C_{13}+C_{44})^2]^{-1/2}$$
$$u_3^4=-(2\gamma_{14}-C_{11}-C_{44})[(2\gamma_{14}-C_{11}-C_{44})^2+(C_{13}+C_{44})^2]^{-1/2}$$
$$u_1^5=(1-A_1/B_1-A_2A_3/B_2B_3)^{-1/2}$$
$$u_2^5=[(A_4/B_3)^2+1+(A_5/B_4)^2]^{-1/2}$$
$$u_3^5=[\sqrt{2}(A_6/B_5)(A_6/B_6+\tfrac{1}{2})+1]^{-1/2}$$
$$u_1^6=(1-A_7/B_7-A_8A_9/B_8B_9)^{-1/2}$$
$$u_2^6=[(A_{10}/B_9)^2+1+(A_{11}/B_{10})^2]^{-1/2}$$
$$u_3^6=[\sqrt{2}(A_{12}/B_{11})(A_{12}/B_{12}+\tfrac{1}{2})+1]^{-1/2}$$
$$A_1=(C_{11}+C_{44}+2C_{66}-4\gamma_{16})(3C_{44}+C_{33}-4\gamma_{16})-\sqrt{2}(C_{13}+C_{44})^2$$
$$B_1=2(C_{13}+C_{44})^2+(C_{12}+C_{66})(3C_{44}+C_{33}-4\gamma_{16})$$
$$A_2=(C_{11}+C_{33}+2C_{66}-4\gamma_{16})(3C_{44}+C_{33}-4\gamma_{16})-\sqrt{2}(C_{13}+C_{44})^2$$
$$B_2=(1/\sqrt{2})(3C_{44}+C_{33}-4\gamma_{16})(C_{12}+C_{66})-(C_{13}+C_{44})^2$$
$$A_3=(2C_{11}+C_{44}+C_{66}-4\gamma_{16})(C_{13}+C_{44})-\sqrt{2}(C_{12}+C_{66})(C_{13}+C_{44})$$
$$B_3=-(C_{11}+C_{33}+2C_{66}-4\gamma_{16})(3C_{44}+C_{33}-4\gamma_{16})+\sqrt{2}(C_{13}+C_{44})^2$$
$$A_4=2(C_{13}+C_{44})^2-2(C_{12}+C_{66})(3C_{44}+C_{33}-4\gamma_{16})$$
$$B_4=(1/\sqrt{2})(3C_{44}+C_{33})(C_{12}+C_{66})-(C_{13}+C_{44})^2$$
$$A_5=(2C_{11}+C_{44}+C_{66}-4\gamma_{16})(C_{13}+C_{44})-\sqrt{2}(C_{13}+C_{44})(C_{12}+C_{66})$$
$$B_5=(C_{11}+C_{33}+2C_{66}-4\gamma_{16})(3C_{44}+C_{33}-4\gamma_{16})-\sqrt{2}(C_{13}+C_{44})^2$$
$$A_6=(3C_{44}+C_{33}-4\gamma_{16})(C_{12}+C_{66})-(C_{13}+C_{44})^2$$
$$B_6=(2C_{11}+C_{44}+C_{66}-4\gamma_{16})(C_{13}+C_{44})-\sqrt{2}(C_{13}+C_{44})(C_{12}+C_{66})$$
$$A_7=(C_{11}+C_{44}+2C_{66}-4\gamma_{17})(3C_{44}+C_{33}-4\gamma_{17})-\sqrt{2}(C_{13}+C_{44})^2$$
$$B_7=2(C_{13}+C_{44})^2+(C_{12}+C_{66})(3C_{44}+C_{33}-4\gamma_{17})$$
$$A_8=(C_{11}+C_{33}+2C_{66}-4\gamma_{17})(3C_{44}+C_{33}-4\gamma_{17})-\sqrt{2}(C_{13}+C_{44})^2$$
$$B_8=(1/\sqrt{2})(3C_{44}+C_{33}-4\gamma_{17})(C_{12}+C_{66})-(C_{13}+C_{44})^2$$
$$A_9=(2C_{11}+C_{44}+C_{66}-4\gamma_{17})(C_{13}+C_{44})-\sqrt{2}(C_{12}+C_{66})(C_{13}+C_{44})$$
$$B_9=-(C_{11}+C_{33}+2C_{66}-4\gamma_{17})(3C_{44}+C_{33}-4\gamma_{17})+\sqrt{2}(C_{13}+C_{44})^2$$
$$A_{10}=2(C_{13}+C_{44})^2-2(C_{12}+C_{66})(3C_{44}+C_{33}-4\gamma_{17})$$
$$B_{10}=(1/\sqrt{2})(3C_{44}+C_{33})(C_{12}+C_{66})-(C_{13}+C_{44})^2$$
$$A_{11}=(2C_{11}+C_{44}+C_{66}-4\gamma_{17})(C_{13}+C_{44})-\sqrt{2}(C_{13}+C_{44})(C_{12}+C_{66})$$
$$B_{11}=(C_{11}+C_{33}+2C_{66}-4\gamma_{17})(3C_{44}+C_{33}-4\gamma_{16})-\sqrt{2}(C_{13}+C_{44})^2$$
$$A_{12}=(3C_{44}+C_{33}-4\gamma_{17})(C_{12}+C_{66})-(C_{13}+C_{44})^2$$
$$B_{12}=(2C_{11}+C_{44}+C_{66}-4\gamma_{17})(C_{13}+C_{44})-\sqrt{2}(C_{13}+C_{44})(C_{12}+C_{66})$$

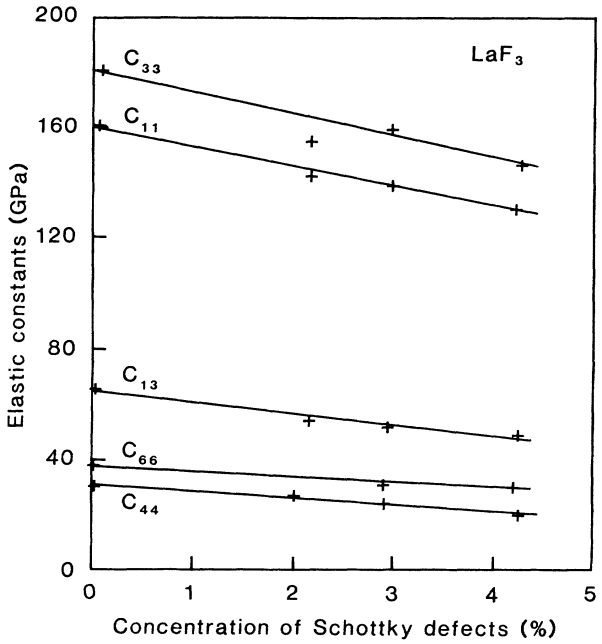

FIG. 8. The calculated change of elastic constants of LaF_3 with increasing concentration of Schottky disorder.

centration of defects or reduce with an increase in the separation of defects.

V. DISCUSSION

The temperature variation of elastic constants of LaF_3 show two regions of interest which are normally observed in fluorite[7] and antifluorite structured compounds.[31] First a linear change occurs up to about 1100 K. The temperature gradients of the measured and calculated elastic constants (Table IV) compare favorably. Since theoretical calculations are based on the quasiharmonic approximation, the corresponding linear changes in the measured elastic constants may be attributed to lattice expansion. Garber and Granato[32] used a similar argument to account for such changes in alkali halides. Secondly, a pronounced reduction of frequencies and elastic constants occurs above 1150 K (it should be noted that the linear behavior persists up to the melting point in alkali halides.) The anomaly in elastic constants starts at the temperature where substantial increases in the excess specific-heat capacity and the ionic conductivity begin. The combination of these phenomena signal the onset of a diffuse transition to a disordered superionic state in analogy with the fluorite structured compounds.

Although anharmonicity is associated with all vibrational modes in solids, it is possible that extreme anharmonicity may develop for specific vibrational modes with increasing temperature, leading to an enhanced level of displacement of atoms from their normal lattice sites. Such vibrational modes would give rise to thermally induced lattice defects, and a distinction between the effects of point defect formation and anharmonicity is not always clear cut. We consider, however, that defect generation is the predominant mechanism responsible for the superionic transition in LaF_3. A comparison of computed elastic constants and those measured by Brillouin scattering provides valuable insights into the dominant mechanisms and species.

The controversy regarding the predominant type of disorder in LaF_3 was referred to in the Introduction. In our simulation studies, the presence of both anion Frenkel and Schottky defects reduced the majority of elastic constants in LaF_3. However, a comparison of the experimental and calculated relative changes in elastic constants, in Table V, favors the Frenkel model. In particular the anomalous behavior of C_{44} is reproduced reasonably well by this model. This consistency, together with a reported lower formation energy for Frenkel than for Schottky disorder,[21] suggests a prevalence of the former defect species in the superionic phase. However, the presence of limited Schottky disorder cannot be ruled out on the basis of lattice parameter and dilatation results.[22]

Other important information derived from the present study is an estimate of the level of disorder in the superionic phase. In Table V we note that most experimental changes of elastic constants at 1400 K are close to those calculated for 2% of Frenkel disorder. It might be argued that concentrations of Schottky disorder other than 2% would yield values which are more consistent with the experimental outcome. However, certain elastic constants, especially C_{13} and C_{66}, are already in agreement with experiment at a 2% concentration of Schottky defects. Hence changing the defect content to force an agreement with other constants will immediately result in a mismatch in C_{13} and C_{66}. Furthermore, the behavior of C_{44} is at variance with the predictions of the Schottky model: indeed, a negligibly small concentration of Schottky disorder will be required to approach the behavior of C_{44}. It is seen, therefore, that the experimental determination of the complete set of elastic constants as a function of temperature has assisted greatly in the interpretation of our theoretical calculations to favor the Frenkel model.

It is further noted from Table IV that the interaction energy of defects rises with increasing content of defects in the lattice. Such interaction reduces the formation energy of defects and is in accord with the model of the diffuse transition discussed in the Introduction. It is clear that there are many features of the current work on LaF_3 in common with that on fluorite-structured compounds. In the latter, neutron scattering and computer simulations studies[33,34] have shown the prominent note played by clusters, formed by defect interactions, influencing features associated with the superionic phase. Studies of this nature in LaF_3 will be of great value.

ACKNOWLEDGMENTS

The authors are grateful to Dr. R. A. Jackson for valuable discussions. One of us (P.E.N.) would especially like to thank the University of Keele for their kind hospitality and the British Council for research support.

APPENDIX

We now present Table VII.

[1]C. R. A. Catlow, Solid State Ion. **8**, 89 (1983).
[2]C. R. A. Catlow, Annu. Rev. Mater. Sci. **16**, 517 (1986).
[3]M. J. Gillan, Physica B+C **131**, 157 (1985).
[4]D. Dasgupta, J. Phys. C **21**, L1011 (1988).
[5]A. V. Chadwick, Solid State Ion. **8**, 209 (1983).
[6]W. Hayes, Contemp. Phys. **27**, 519 (1986).
[7]C. R. A. Catlow, J. D. Comins, F. A. Germano, R. T. Harley, and W. Hayes, J. Phys. C **11**, 3197 (1978).
[8]C. R. A. Catlow, J. D. Comins, F. A. Germano, R. T. Harley, W. Hayes, and I. B. Owen, J. Phys. C **14**, 329 (1981).
[9]P. E. Ngoepe and J. D. Comins, J. Phys. C **19**, L267 (1986).
[10]P. E. Ngoepe and J. D. Comins, Cryst. Lattice Defects Amorph. Mater. **15**, 317 (1987).
[11]R. Laiho, M. Lakkisto, and T. Levola, Philos. Mag. **47**, 235 (1983).
[12]P. E. Ngoepe, J. D. Comins, and A. G. Every, Phys. Rev. B **34**, 8153 (1986).
[13]P. E. Ngoepe and J. D. Comins, Phys. Rev. Lett. **61**, 978 (1988).
[14]A. V. Chadwick, D. S. Hope, G. A. Jaroszkiewicz, and J. H. Strange, in *Fast Ion Transport in Solids*, edited by P. Vashista, J. N. Mundy, and G. K. Shenoy (Elsevier, Amsterdam, 1979), p. 683.
[15]J. Schoonman, G. Overhuizen, and K. E. D. Wapenaar, Solid State Ion. **1**, 211 (1980).
[16]K. Lee and A. Sher, Phys. Rev. Lett. **14**, 1027 (1965).
[17]M. Goldman and L. Shen, Phys. Rev. **144**, 321 (1966).
[18]E. Ildstad, I. Svare, and T. A. Fjeldly, Phys. Status Solidi A **43**, K65 (1977).
[19]G. A. Jaroszkiewicz and J. H. Strange, J. Phys. C **18**, 2331 (1985).
[20]A. F. Aalders, A. Polman, A. F. M. Arts, and H. W. de Wyn, Solid State Ion, **9**, and **10**, 593 (1983).
[21]W. M. Jordan and C. R. A. Catlow, Cryst. Lattice Defects Amorph. Mater. **15**, 81 (1987).
[22]A. Sher, R. Solomon, K. Lee, and M. W. Muller, Phys. Rev. **144**, 593 (1966).
[23]J.R. Igel, M. C. Winterling, J. J. Fontanella, A. V. Chadwick, C. G. Andeen, and V. E. Bean, J. Phys. C **15**, 7215 (1982).
[24]A. V. Chadwick, K. W. Flack, and P. E. Ngoepe, Solid State Ion, (to be published).
[25]W. G. Lyon, D. W. Osborne, H. E. Flotow, F. Grandjean, W. Hubbard, and G. K. Johnson, J. Chem. Phys. **69**, 167 (1978).
[26]C. de Rango, G. Tsoucaris, and C. Zelwer, Acad. Sci. Ser. C **263**, 64 (1966).
[27]A. Zalkin and D. H. Templeton, Acta Crystallogr. B **41**, 91 (1985).
[28]C. R. A. Catlow and M. J. Norgett, AERE Harwell Report M. 2763, 1978 (unpublished).
[29]B. G. Dick and A. W. Overhauser, Phys. Rev. **112**, 90 (1958).
[30]P. E. Ngoepe, Ph.D. thesis, University of the Witwatersrand, Johannesburg, 1987 (unpublished).
[31]T. W. D. Farley, M. A. Hackett, W. Hayes, S. Hull, M. T. Hutchings, R. Ward, and M. Alba, Solid State Ion. Diffus. React. **28–30**, 189 (1989).
[32]J. A. Garber and A. V. Granato, Phys. Rev. B **11**, 3990 (1975).
[33]M. T. Hutchings, K. Clausen, M. H. Dickens, W. Hayes, J. K. Kjems, P. G. Schnabel, and C. Smith, J. Phys. C **17**, 3903 (1984).
[34]C. R. A. Catlow and W. Hayes, J. Phys. C **15**, L9 (1982).